A CFD Based Parametric Analysis of S-shaped Inlet for a Novel Blended Wing Body Aircraft

Gangoli Rao, Arvind; Sharma, A.; van Dijk, Reinier

DOI
10.2139/ssrn.3101299

Publication date
2017

Document Version
Accepted author manuscript

Published in
International conference on Advances in Thermal Systems, Materials and Design Engineering

A CFD Based Parametric Analysis of S-shaped Inlet for a Novel Blended Wing Body Aircraft

Arvind Gangoli Rao, Abhishek Sharma, Reinier van Dijk

ABSTRACT- **The Advisory Council for Aeronautics Research in Europe (ACARE) has set an ambitious array of objectives to be accomplished by 2050 for civil aviation. It is often claimed that complying with those targets will not require evolution but, rather, revolution. If the growth in aviation has to be sustained in the future, then we must come up with radical aircraft and engine configurations which can meet the demands of future aviation.**

The AHEAD project (co-funded by the European Commission) investigated a novel multi-fuel blended wing body aircraft with a unique propulsion system to address the challenges of the future. The engine for this aircraft uses an embedded hybrid engine exploiting the boundary layer ingestion technique to increase the propulsive efficiency.

Two major consequences of BLI are vital in this regard. Namely, loss of total pressure recovery and increased total pressure distortion at the Aerodynamic Interface Plane (AIP) or the engine fan-face. Hence, the inlet performance is measured by the total Pressure Recovery Factor (PRF) and Distortion Coefficient (DC_{60}). The current research work aims to design an embedded inlet on a Blended Wing Body (BWB) aircraft that produces maximum value of PRF and minimum DC_{60}.

The aim of this research is to investigate the S-shaped inlet to understand the effect of various geometrical parameters on its performance. The Knowledge Based Engineering platform ParaPy is used to parametrize the S-shaped inlet and generate a variety of inlet geometries and volume meshes. These different variants were analysed using the Ansys® CFD code.

I. INTRODUCTION

WITH global warming becoming one of the major problems faced by humankind, emissions from aircraft can no longer be ignored [1,2]. Hence, there is an urgent need to reduce the emission of CO_2, NOx, CO and other pollutants. Air traffic has been growing at around 5% every year for last few decades and the forecast suggests that it will continue to grow at the same rate in the coming decades [3].

It is anticipated that the emission norms will become more stringent in the coming years with the consequent need to reduce pollutants level drastically. The anticipated reduction at various fronts (noise, air pollution and fuel consumption) required to meet the future challenges (by the year 2050), as envisioned by the ACARE are shown in Fig. 1. [4]. It can be observed that the objective for the year 2050 is to reduce CO2 emission by 75%, NOx emission by 90%, and noise emission by 65%. This objective can only be achieved by dramatic improvement of both aero engine and aircraft. Incremental changes to the current aircraft and engine will not result in substantial improvements in emission reduction.

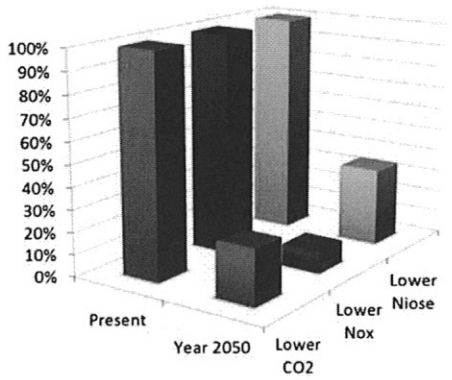

Fig. 1: ACARE vision for Europe

As far as the engine is concerned, the SFC can be reduced by increasing the thermal and propulsive efficiency. Till now the propulsive efficiency was increased by increasing the bypass ratio of the engine. However, this improvement is limited due to constraints of increased engine weight and size. Within the AHEAD project sponsored by the European Commission (FP7), a new aircraft concept called Multi-Fuel Blended Wing Body (MF-BWB) aircraft, and a new type of propulsion system for this aircraft (called the hybrid engine) have been proposed [4-6]. The superior aerodynamic features of the MF-BWB aircraft make it possible to store cryogenic fuels (like LNG or LH2) without incurring serve aerodynamic penalties. The hybrid engine is mounted on the upper aft part of the MF-BWB aircraft such that the propulsion system could benefit from the Boundary Layer Ingestion (BLI).

"The research leading to these results has received funding from the European Union Seventh Framework Programme (FP7/2007-2013) under grant agreement n° 284636. The authors would like to acknowledge the support of all the partners of this AHEAD project. The authors are grateful to ParaPy B.V. for providing the ParaPy software for this research work".

Dr. Arvind Gangoli Rao is an Associate Professor at the faculty of aerospace engineering, Delft University of Technology, The Netherlands (e-mail: A.Gangolirao@tudelft.nl).

Abhishek Sharma worked on this project as a graduate student and presently working as a Mechatronics Design Engineer at ASML, Netherlands (email: abhishek.sharma-asjm@asml.com).

Reinier van Dijk is the CEO and Founder of ParaPy B.V. He is also with the faculty of aerospace engineering at Delft University of Technology, Delft, The Netherlands (e-mail: Reinier@parapy.nl).

In the BLI concept, the engine propulsive efficiency can be increased without increasing the bypass ratio due to lowering of the ram drag and utilization of the wake kinetic energy [7, 8]. The BLI has other advantages, like reduction in the nacelle wetted area and engine noise shielding. These advantages help in reducing the noise footprint of the aircraft substantially.

II. NOMENCLATURE

A. Roman Symbols

AR	Inlet Aspect Ratio	[-]
A_F	Fan Area	[m^2]
a	Major axis length of elliptical inlet face	[m]
b	Semi-minor axis length of elliptical	[m]
CR	Contraction Ratio	[-]
$C_{Pt,loss}$	Total pressure loss coefficient	[-]
DC_{60}	Distortion Coefficient	[-]
D_{fan}	Diameter of Engine Fan	[m]
H	Height of Duct	[m]
L	Length of Duct	[m]
M	Mach Number	[-]
M_D	Drag Rise Mach Number	[-]
MFR_{crit}	Critical Mass Flow Ratio	[-]
$\dot{m}$	Mass Flow Rate	[kg/s]
P_m	Area averaged total pressure fan face	[Pa]
PRF	Pressure Recovery Factor	[-]
q	Dynamic Pressure	[Pa]
Re	Reynold's Number	[-]
y^+	Non-dimensional Wall Distance	[-]

B. Abbreviation

ACARE	Advisory Council for Aviation Research and innovation in Europe
AHEAD	Advanced Hybrid Engines for Aircraft Development
AIP	Aerodynamic Interface Plane
BLI	Boundary Layer Ingestion
CFD	Computational Fluid Dynamics
DC_{60}	Circumferential Distortion for 60 deg sector
FPR	Fan pressure ratio
KBE	Knowledge Based Engineering
LH2	Liquid Hydrogen
LNG	Liquefied Natural Gas
MFBWB	Multi-fuel Blended Wing Body
PAI	Propulsion Airframe Integration
PFC	Passive Flow Control
MDO	Multidisciplinary Design Optimization
RANS	Reynold's Averaged Navier Stokes
SFC	Specific Fuel Consumption
SST	Shear Stress Transport

III. THE MULTI FUEL BLENDED WING BODY

Cryogenic fuels should be stored in insulated cylindrical or spherical tanks. This makes it challenging for conventional aircraft. The volume available in the wing can no longer be utilized for storing fuel. Figure 2 shows an aircraft that was designed in the "Cryoplane" project to store LH_2 in insulated tanks within the fuselage of the aircraft [9]. However, due to the lower volumetric energy density of LH2, the fuselage diameter is increased substantially, which in turn increases the aircraft drag and thereby the required thrust. This has an adverse effect on the overall fuel burn for the mission and increases the energy consumption per passenger between 8-20%, depending on the mission range [10].

Fig. 2: Bubble Fuselage Concept [9]

As compared to a conventional aircraft, the BWB concept is more promising for alternative fuels. The BWB aircraft has been studied by many researchers around the world. More space is available within BWB aircraft in which cylindrical fuel tanks can be stored. A novel multi fuel-BWB concept was investigated by TU Delft. The proposed MF-BWB configuration can be seen in Fig. 3 [11]. The features of the aircraft are listed below.

- Carrying around 300 passengers
- Range of 14,000 km
- Ability to carry multiple-fuel, such as LNG /LH2 and Kerosene
- Utilizing Boundary Layer Ingestion (BLI) technology
- Ability to reduce CO_2, NO_x and noise emissions

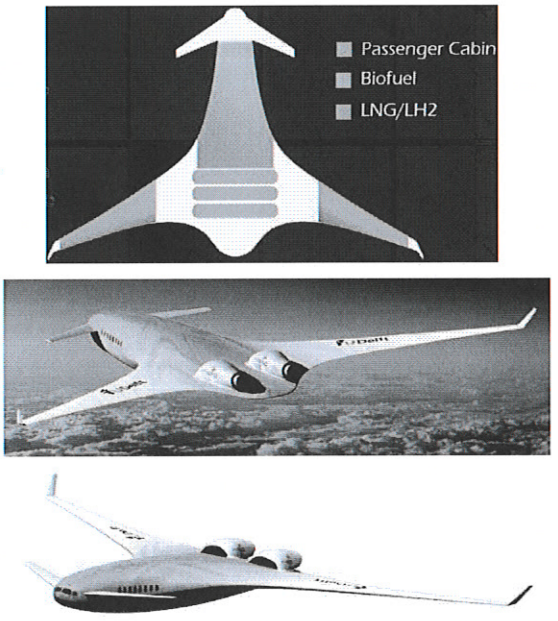

Fig. 3: Schematic of the AHEAD Multi-Fuel BWB Aircraft Design [11]

IV. THE HYBRID ENGINE CONCEPT

Although the proposed MF-BWB concept seems very promising, it won't be able to meet the challenges alone without improvement of the propulsion system. Over the years, gas turbine engines have improved significantly from the early pure jets to the current high bypass turbofan engines. The aspiration to make these engines stronger, lighter and more efficient has kept scientists and engineers occupied for decades, and continue to this day. Traditional ways of increasing engine efficiency include increasing the BPR, OPR, and TIT, [12, 13]. However, these parameters are reaching their limits. Increasing BPR leads to increase in the engine weight and engine diameter, thereby increasing the drag and reducing the ground clearance. Increasing OPR leads to heavy and long engines. The TIT is mainly limited by turbine material and cooling technology level.

In order to exploit this unique opportunity provided by the proposed MF-BWB aircraft, a novel engine concept has been conceived. The schematic of the engine is presented in Fig. 4 [6,7].

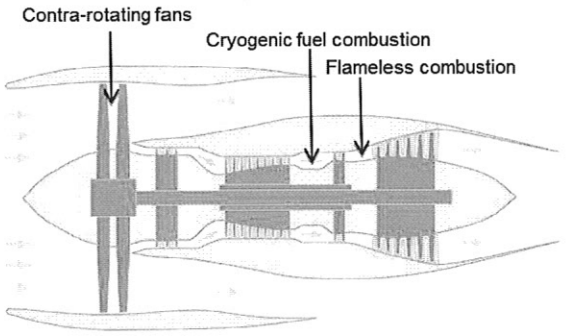

Fig. 4: Schematic of Hybrid Engine

The proposed hybrid engine is a combination of several technologies. The main features of this aircraft engine are shown as below:

- **Counter rotating fans:** to better sustain the non-uniform inflow caused by Boundary Layer Ingestion (BLI) techniques [14].
- **Dual Combustion Chamber**: The first combustion chamber (located between the HPC and HPT) burns cryogenic fuel (such as LH2/LNG) in a vaporized state [15], whereas, the second combustor is an Inter-stage Turbine Burner (ITB) which uses kerosene/biofuels in the flameless combustion mode [16], and is beneficial from NOx emission perspective.
- **Bleed Air Cooling System**: This system allows exploiting the cooling capacity provided by the cryogenic fuel to enhance the thermodynamic efficiency of the cycle by reducing the amount of compressor bleed air required for turbine cooling [17].

The implementation of these novel aircraft and engine technologies have the potential to reduce CO_2 and NO_x emissions substantially to meet the ACARE goals.

V. THE BOUNDARY LAYER INGESTION INLET

The aircraft engine integration on a BWB can be achieved either by mounting the engines on a pylon or by embedding the engine in the fuselage. Podded engines ingest clean airflow, but have the disadvantages of increased weight, fuel burn and drag. Whereas embedding the engines in the fuselage implies ingestion of the boundary layer. According to studies conducted in the domain of BLI, it is known that propulsive efficiency can be increased if part or all of the propulsive fluid comes from the wake of the aircraft [18, 19]. Boundary layer ingested into the engines consists of the low momentum fluid developed over the fuselage surface. Due to these losses, the inlet suffers a lower mass averaged stagnation pressure at the lip. Figure 5 shows the inlet velocity profile for an embedded engine configuration.

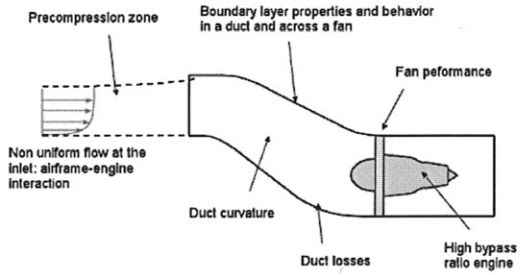

Fig. 5: Inlet velocity profile in an embedded engine configuration [20]

There are several problems that arise due to BLI on a BWB, the major ones are:

- Distortion at AIP
- Secondary flow in the S-Duct
- Loss of total pressure recovery

A. Distortion at AIP:

Distortion at the engine fan face is one of the major causes of loss in engine efficiency. The efficiency of a turbofan engine depends largely on clean and uniform airflow conditions. Due to BLI, there are several non-uniformities in pressure and velocity flow field in the duct. These fluctuations at the AIP lead to unsteady loading of the fan blades and reduce the efficiency and operating stall margin. Moreover, due to increased loading cycles, the life cycle of engine components is reduced [21].

The industry has set certain standards to keep the distortion levels within limits. Distortion Coefficient (DC_{60}) is one such standard in which, q is the dynamic pressure, $P_{t,m}$ is the average total pressure over the fan face area and P_{60min} is the minimum area-averaged total pressure on any 60° sector of the fan face. For civilian applications, acceptable levels of DC_{60} occur below 0.1 and for military applications, it occurs below 0.2 [22].

$$DC_{60} = \frac{P_{t,m} - P_{60,\min}}{q_\infty} \qquad (1)$$

B. Secondary flow in the S-Duct:

Due to the shape of the S-Duct, the flow entering the duct is highly distorted due to large vortex pair formation inside the duct. At the first bend, the flow accelerates, since the bottom part is turned away from the flow, which creates a local static pressure drop [23]. The boundary layer then becomes prone to separation due to the resulting adverse pressure gradient.

After the flow exits the first bend, the pressure outside becomes higher than the pressure inside of the bend, hence the flow experiences a transverse pressure gradient. As a result, a large accumulation of boundary layer takes places and the boundary layer is pulled towards the core flow. This causes a lift-off effect, forming two counter-rotating vortices which are pulled towards the core flow [24].

There are other causes of secondary flow formation within an S-Duct. The corners of the inlet face along the duct, where the duct lip meets the airframe surface, also experience secondary flow formation. The flow around the corners accelerates around the inlet lip, creating a horseshoe vortex [25], as shown in Fig 6.

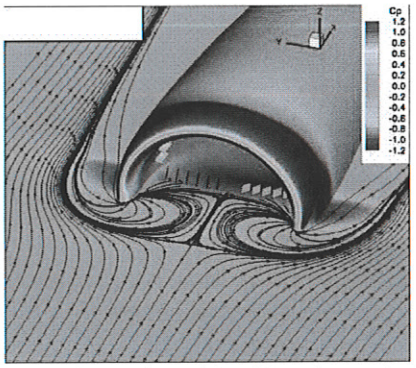

Fig. 6: Secondary flow vortices at inlet airframe intersection [25]

C. Loss of total pressure recovery:

Another factor, which contributes largely to intake efficiency, is the Pressure Recovery Factor (PRF). This is defined by the equation:

$$PRF = \frac{P_{t2}}{P_{t0}} \qquad (2)$$

Here, P_{t2} represents total pressure at the AIP and P_{t0} is total pressure at the inlet. The PRF is a measure of efficiency at which kinetic energy of the incoming flow is converted into pressure energy. For increasing the total efficiency, the PRF should be close to unity.

However, it is known that ingesting airframe boundary layer results in average total pressure loss at the AIP. At low Mach numbers, it is difficult to detect changes in total pressure loss for different flow conditions. Therefore, sometimes a non-dimensional total pressure loss coefficient is used to measure the pressure recovery performance at the fan [26].

$$C_{PtLoss} = \frac{P_{t\infty} - P_{tAvg}}{q_{\infty}} \qquad (2)$$

VI. THE S-SHAPED INLET FOR BLI

While designing an inlet for BLI, the following criteria should be aimed at:

- Low total pressure distortion at the AIP
- High total pressure recovery at the AIP
- High BLI for high wake recovery
- Acceptable velocity at the engine fan-face for high pressure rise across compressor
- Minimal secondary flow formation inside the S-duct
- Low overall drag

The design of the S-Duct depends on a number of geometrical parameters, some of which are listed as follows:

- Inlet duct offset
- Curvature of the two bends (spline shape)
- Area Ratio (Fan area/Inlet throat area)
- Inlet aspect ratio
- Length of duct
- Height of duct
- Percentage of BLI

Mentioned above are some of the major parameters that affect the design of an S-Duct inlet. However, the scope of this work is limited to testing by geometrical variations in length, height and aspect ratio of the duct.

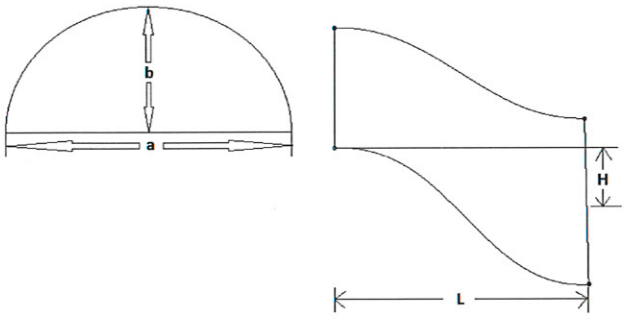

Fig. 7: Geometrical parameters of the S-shaped inlet

VII. THE NUMERICAL SETUP

The software used for solving the fluid dynamics and subsequent analysis was ANSYS CFX. The underlying numerical algorithms are solved for a number of boundary conditions to capture the flow physics inside the inlet. Various turbulence models are available for approximating the complex flow phenomenon, namely Spalart-Allmaras model, k-ε model, k-ω model and the Shear Stress Transport (SST) model. The k-ε model is a widely used turbulence model that is relatively good at capturing the BL. The standard k-ε model is used in the current work for modelling the turbulence. The k-ε model consists of 2 transport equations which describe the turbulence:

- *Turbulent Kinetic Energy (k)*: determines the energy in the turbulence
- *Turbulence Dissipation Rate (ε)*: determines the rate of dissipation of the turbulent kinetic energy

The Knowledge Based Engineering platform ParaPy was used to develop a parametric S-Duct model. This model could automatically generate the large number of geometries and grids required to study the influence of shape parameters, like length, height and aspect ratio, on the flowfield at the AIP.

ParaPy is designed for automation of routine engineering tasks, which otherwise require a large amount of time, including CAD modelling, meshing, CAE pre- and post-processing. The ParaPy language allows engineers to write custom applications that capture and re-use the rules and knowledge underlying such routine tasks [27]. Given its high degree of automation, ParaPy is an enabler of (multi-disciplinary) optimization studies like the one conducted in this research.

The ParaPy core language component is built on top of Python making it easy to use and accessible to engineers with relative little programming experience. ParaPy's grammar guides engineers in creating a structured product model composing multiple objects, each with their own inputs and outputs, and with parametric interdependencies. For example, the S-Duct model composes objects like `Inlet`, `Outlet`, `Path`, `Loft` and `MeshGenerator`. Examples of inputs are `major_radius` or `max_element_size`.

The language also provides an efficient computation engine that caches (i.e. memorizes) values to avoid (expensive) re-computation, but also invalidates these caches as parameters change by active dependency tracking. Moreover, ParaPy ensures lazy evaluation, i.e. only computing those parts of a product model that are required to return the value of a parameter of interest. This guarantees a scalable model that can naturally evolve as the product grows more complex and multiple disciplines are coupled [28].

The geometry library provides a set of roughly 200 objects that allow an engineer to express the intent behind the 3d model generation. To generate the 3d model, ParaPy has bindings to the OpenCascade (OCCT) geometry kernel (written in C++). The ParaPy geometry library has been designed to insulate the engineer from the complexity of a low-level kernel like OCCT, allowing him/her to model intentions on a significantly higher abstraction level making it more accessible and saving application development time.

Similarly, the ParaPy meshing library contains dozens of objects to assign grid generation algorithms and quality controls to the 3d model. It wraps the Salome meshing suite on the back-end for this purpose. The assignment of algorithms and quality controls is *associative*, meaning that any changes to the geometry will reflect in a change of the grid. In this research, the meshing library allowed for the automatic generation of grids that were ready to be fed into ANSYS CFX for analysis.

As shown in Fig. 8., the mesh features an unstructured core region of tetrahedral elements and a prismatic wall region to accurately capture the boundary layer (gradient). The total number of elements is approximately 600,000 for the smallest duct variant. An unstructured mesh was chosen due to its ease in meshing,

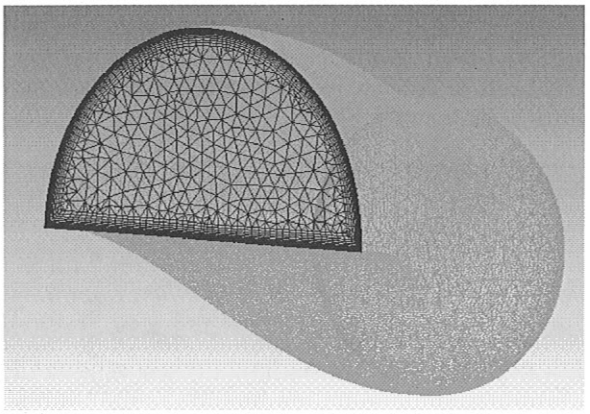

Fig. 8: Mesh topology for an inlet configuration

C. Boundary Conditions:

The boundary conditions for the inlet configurations are defined as follows [29]:

1) Inlet:

The entry of the S-Duct at the semi-elliptical face (shown in Fig. 8) is defined as the inlet. The velocity profile at the location, where the inlet will be embedded, is obtained from the results of the BWB fuselage simulation (shown later) and applied as an inlet to the semi-elliptical entry face of the inlet.

2) Outlet:

The circular face at the exit of the S-Duct is defined as the outlet for the inlet configurations. This circular face is the engine fan-face or AIP. Some of the critical effects of flow inside the S-Duct will be assessed based on results of total pressure distortion and Mach number at the engine fan-face. The diameter of the engine fan face is constant.

3) Wall:

Between the inlet and the outlet, solid wall condition is defined for the cylindrical surface. Flow is considered adiabatic, which means no heat transfer is assumed. The wall is a no-slip boundary condition.

The first stage of testing consisted of a 3D model of a BWB aircraft in clean configuration (without engines). A flow simulation was conducted in order to obtain velocity profiles over aft fuselage at different locations, where the inlet will be embedded. These velocity profiles were applied as inlet boundary conditions to the S-shaped ducts simulated subsequently.

The S-Ducts were tested separately using BWB velocity profiles in order to save computational time, as testing entire BWB configuration with embedded engines for every variation of length, height and aspect ratio was not a feasible option. Figures 9 and 10 show the BWB aircraft in clean

configuration and the velocity profiles at the aft fuselage, where the inlets of the ducts were supposed to start. The main assumption in this analysis is that the engine suction will not affect the BL over the fuselage substantially. It can be seen from Fig 10 that the flow over the fuselage accelerates to a high value because of the curvature of the fuselage. However, towards the aft of the fuselage, the flow velocity starts to decrease as the flow decelerates and the boundary layer becomes thicker.

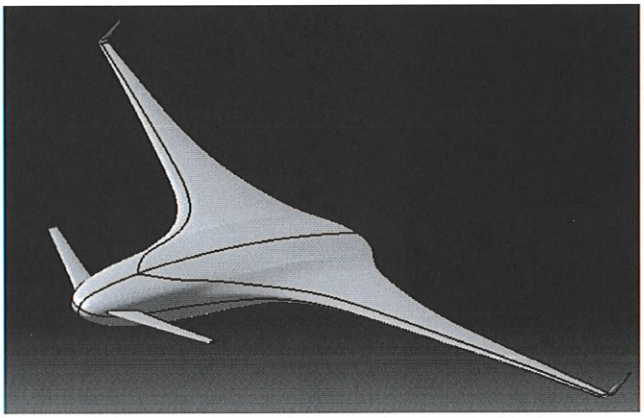

Fig. 9: BWB in clean configuration (without engines) [30]

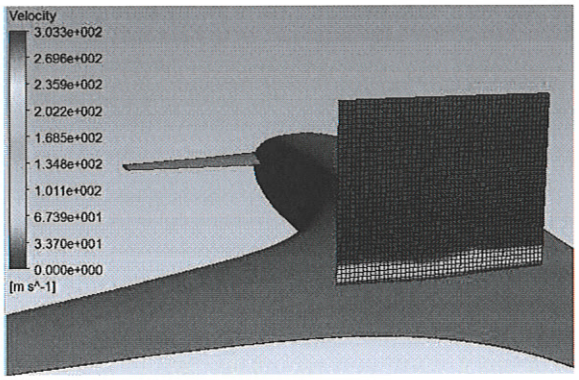

Fig. 10: Velocity profile on the MF-BWB fuselage, used as an inlet boundary condition to the S-shaped inlet.

First, the tests were carried out for the shortest duct length (4.85m) and a given height value (1.052m) and changes were carried out for various aspect ratios. As shown in Table 1 the, aspect ratio was varied from 1 to 2.5. This meant that the inlet became wider as the aspect ratio was increased and consequently the amount of percentage of fuselage boundary layer ingested increased. Variation in aspect ratio is critical in understanding the effect of increasing percentage of BLI. Table 1 shows all the values of aspect ratio, length, and height of duct tested in this work. A combination of these values will determine the most optimum S-Duct inlet configuration.

Table 1
Values of geometrical parameters for testing

Aspect Ratio (AR)	Height of Duct (H)	Length of Duct (L)
1	1.5m	4.85m
1.25	1.052m	5.65m
1.5	0.7m	6.46m
1.75	0.3m	7.27m
2		
2.5		

Table 2
Operating Conditions

Flight Regime	**Cruise**
Altitude	10000 m
Mach Number	0.82
Free-stream Velocity	279 m/s
Density of Air	0.41 kg/m^3

After an optimum value of aspect ratio was chosen, height was varied, keeping the duct length constant for the chosen aspect ratio. Subsequently, after a conclusion on the value of height, variation in length indicated the optimum length of the duct required to achieve minimized losses in terms of pressure recovery, distortion and wetted area.

VIII. RESULTS

Figure 10 shows a sampling plane displaying the local velocity profile at a possible inlet integration location. Depending on the length of the inlet, the velocity profiles were obtained and exported to the CFX setups of the S-Ducts to be applied as inlet boundary condition for the same. The investigation was carried out on the S-Duct for varying aspect ratios starting from AR=1. Figure 11 shows the results of total pressure and x-velocity obtained at the engine fan-face or AIP for AR=1 [29].

Figure 11 clearly shows the effect of the formation of a vortex pair at the bottom of the S-Duct. This vortex pair is a part of the secondary flows formed at the second bend of the S-Duct due to the adverse pressure gradient experienced by the low momentum boundary layer, which easily separates and causes a region of recirculation.

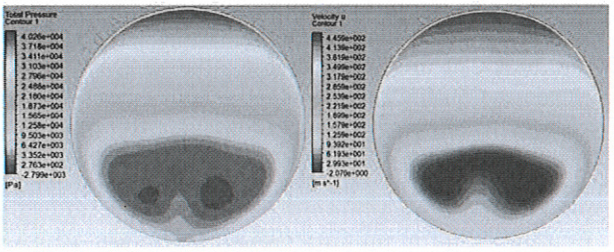

Fig. 11: Total pressure and x-velocity contours at AIP for AR=1

Since the freestream flows on the upper part of the S-Duct experience a favorable pressure gradient, it accelerates and a low static pressure region is created in the upper part. This region of low static pressure lifts the slow-moving boundary layer, causing the formation of the vortex pair at the bottom of the S-Duct. This is shown in detail in Fig 12. The distorted total pressure distribution at the AIP will cause non-uniform loading of the fan, which can lead to vibrations of the fan blade and blade stall. Therefore, it is important to understand the cause of these secondary flows and to improve the design to minimize their formation.

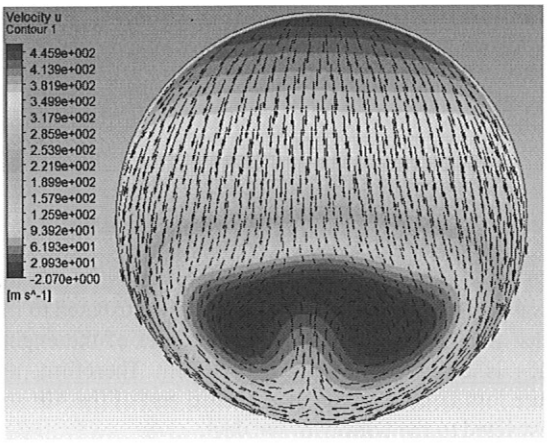

Fig. 12: Tangential flow at the AIP

Figure 12 shows the negative velocity in the region of recirculation, at the bottom of the S-Duct. This region of recirculation adversely affects the total pressure recovery and increases total pressure distortion at the AIP, as will be seen later in this section. It is also seen that the upper limit of x-velocity value is too large (445.9 m/s), which is a consequence of flow acceleration on the top part of the S-Duct. To provide a better understanding of how the flow, Fig. 13 depicts the streamlines over the x-velocity contours to show flow acceleration and point of separation.

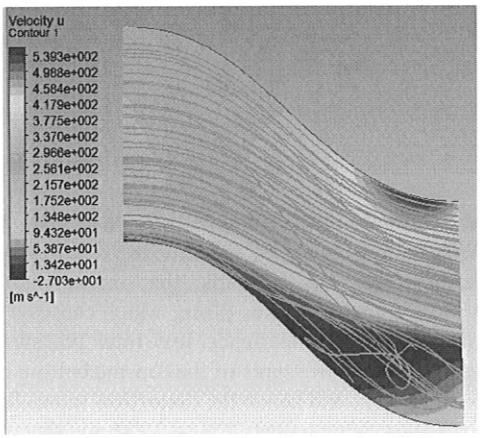

Fig. 13: Streamlines at the mid-plane for AR=1

One reason for this extremely high velocity on the upper part of the duct is the long length of the semi-minor axis of the inlet face for AR=1, which is 3.08m. For low aspect ratios, the inlet face is higher and less wide (See Fig. 7). And since the height is parameterized from center of inlet face to center of AIP and is constant while varying aspect ratio, the only variation in the curvature of the upper spline of the S-Duct comes from the length of the semi-minor axis of the inlet face. For high aspect ratios, the length of the semi-minor axis is low as compared to the length of the major axis of the inlet face, indicating a wider inlet face and hence larger amount of BLI. This shortening of semi-minor axis length of the inlet face with increasing aspect ratio, in turn, reduces the pressure gradient at the upper part of the S-Duct and flow acceleration reduces.

Figure 14 shows boundary layer separation and the region of negative velocity at the bottom part of the duct. The large semi-minor axis length of the inlet face can also be seen at the entry of the S-Duct at the left. The region of recirculation seen in Fig. 14 can be reduced with careful selection of the aspect ratio value, by reducing the height of duct, etc. which will be discussed in subsequently.

To show the difference in upper spline curvature of S-Duct, Fig. 15 shows the mid-plane view of the S-Duct with AR=2.5 (widest inlet with shortest semi-minor axis length). It can be seen from Fig. 15 that the pressure gradient on the upper spline has considerably reduced with increased aspect ratio. This means that the flow on the upper wall of the duct does not accelerate as much as it does for the duct with AR=1. Hence, the static pressure region on the upper wall of the AR=2.5 duct is not as low as for AR=1 duct. However, aspect ratios as large as 2.5 are not desirable due to high pressure loss because of large ingestion of fuselage boundary layer.

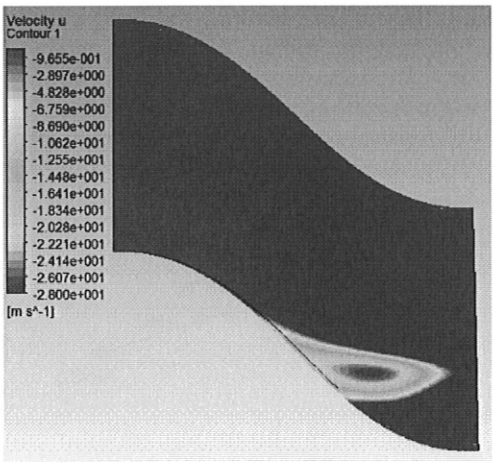

Fig. 14: Mid-plane view of S-Duct (AR=1) showing recirculation region

Pressure recovery is an important criterion in judging inlet performance. Pressure loss in the duct can be due to a number of reasons namely higher surface area of the duct that causes higher wall friction, the formation of secondary

flows in the duct due to flow separation, high vorticity in the boundary layer, increased turbulence, etc.

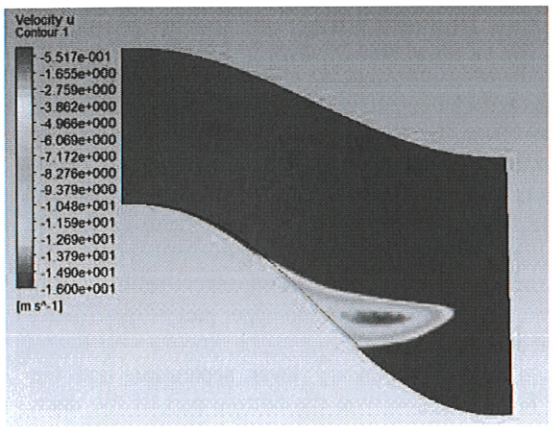

Fig. 15: Mid-plane view of S-Duct with AR=2.5 showing recirculation region

Figure 16 shows the variation of total pressure recovery with increasing BLI. The difference in the values of pressure recovery for different aspect ratios is not significant. However, it is noticeable that the pressure recovery increases up to an aspect ratio of 1.75 and then starts to decrease for very high aspect ratios. This trend can be explained based on the discussion in the previous section regarding the upper spline curvature of the S-Duct. As discussed before, with increasing aspect ratio, the upper spline curvature of the duct reduces, because of which the static pressure region in this part is not low enough to lift up the slow-moving boundary layer on the bottom wall. Hence, pressure loss reduces up till AR=1.75.

Interestingly, this phenomenon is not persistent after AR=1.75. This is mainly because for aspect ratios greater than 1.75, the percentage of BLI becomes too high (43%) relative to the ingested free-stream to maintain a low pressure loss. Also, for aspect ratios greater than 1.75, a major part of the AIP is covered with vortex pair developed inside the duct, which reduces total pressure at the AIP, even though it reduces distortion (explained in the next section).

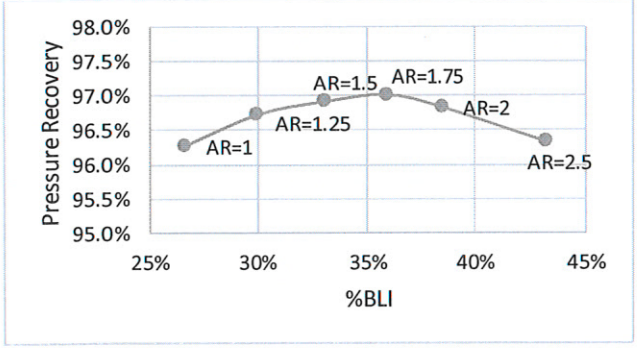

Fig. 16: Variation of Pressure Recovery with the percentage of BLI

Aspect ratio will also influence distortion at the AIP. As the aspect ratio increases, BLI increases and hence more non-uniform flow is ingested by the inlet, which means that the distortion should increase with increasing aspect ratio. This is seen in Fig. 17, where the distortion coefficient, DC_{60}, increases with increasing aspect ratio till AR=1.75.

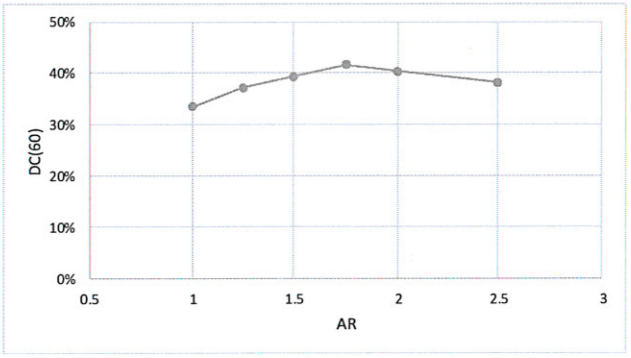

Fig. 17: Variation of DC_{60} with the aspect ratio

In Fig. 17, it can be seen that after an AR of 1.75, the DC_{60} value starts to decrease. This is mainly attributed to the fact that at higher aspect ratios, a large part of the engine fan-face is covered with the vortex pair. Therefore, the pressure loss is now spread over a large part of the AIP and not restricted to the bottom of the duct.

Figure 18 shows the variation of pressure recovery with increasing duct height. The pressure recovery value reduces from 97.7% to 96.4%. with increasing duct height.

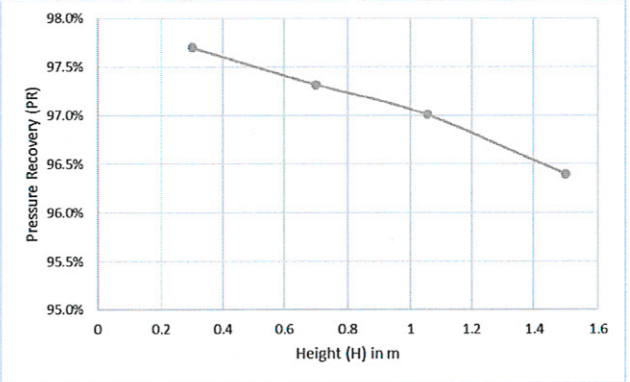

Fig. 18: Variation of pressure recovery with duct height

The effect of variation in duct height influences distortion at the AIP. With increasing height, the boundary layer separation moves further upstream towards the throat and large secondary flow formation takes place, which causes a major portion of the AIP to experience low total pressure. The difference in the total pressures of the top and bottom half of the AIP is significant and hence the distortion values linearly increase with increasing height. Figure 19 shows that there is approximately a 15% increase in the value of DC_{60} as the height increases from 0.3m to 1.5m. Hence, H=0.3m is chosen

as the preferred height value for further testing with variation in duct length.

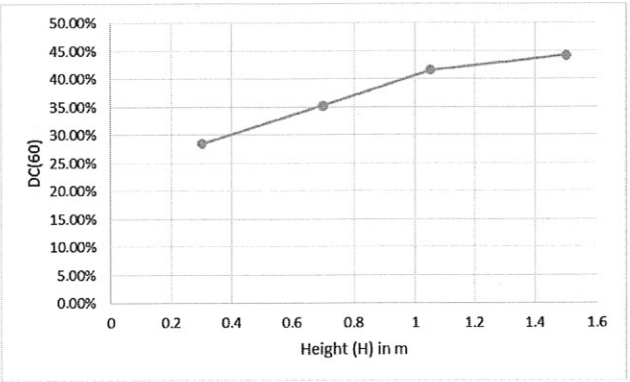

Fig. 19: Variation of DC_{60} with duct height

The duct length plays a crucial role in the overall performance of the inlet. Four different duct lengths were tested ranging from 4.85m to 7.27m. It is quite clear from Fig. 20 that the total pressure on outlet decreases as the duct length increases. As discussed before, this is mainly due to pressure losses resulting from the larger wetted surface area for the longer duct. This, in turn, means that the pressure recovery will get reduced as the length of duct is increased.

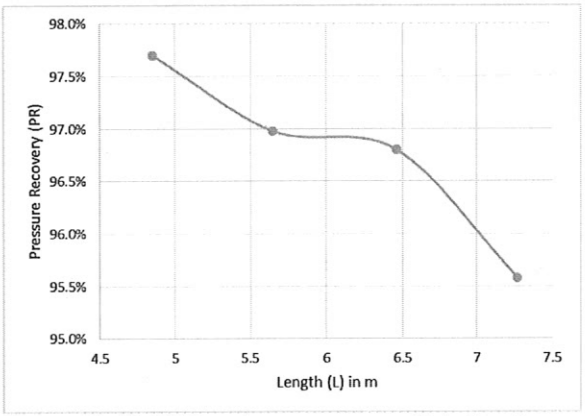

Fig. 20: Variation of pressure recovery with duct length

The increase in length causes higher pressure losses in the boundary layer as compared to the freestream. This causes a large difference in pressure loss in the upper half of the AIP (affected by free-stream without major losses) and the bottom half where the low momentum boundary layer imparts low pressure. This difference in pressures gives rise to a large distortion value for the longer ducts. From Fig. 21, it is evident that the shortest duct gives the best performance with a DC_{60} value of 28%.

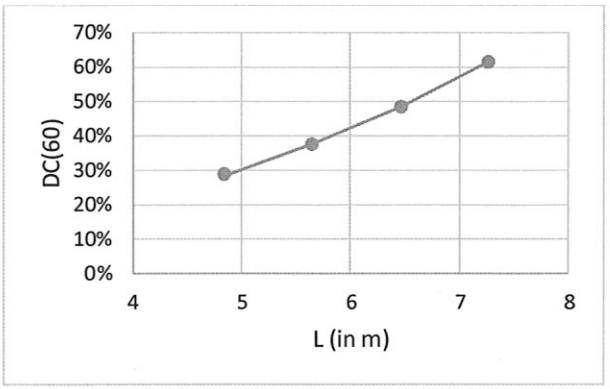

Fig. 21: Variation of DC_{60} with duct length

From the conclusions on length, height and inlet aspect ratio results, so far the inlet with the best performance (PR = 97.7% and DC_{60} = 28.45%) has the following dimensions: H=0.3m, L=4.85m and AR=1.75. Figures 22 and 23 show the flow development and streamlines inside the S-duct obtained from testing, respectively.

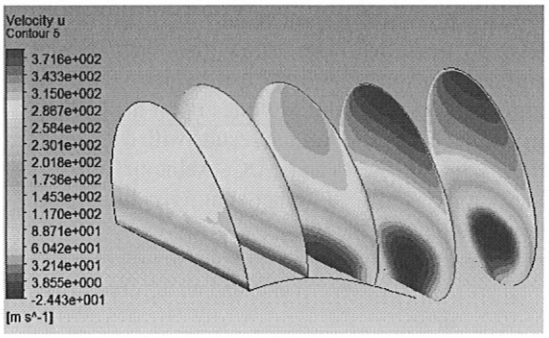

Fig. 22: Flow development inside the S-duct obtained from testing of geometrical parameters

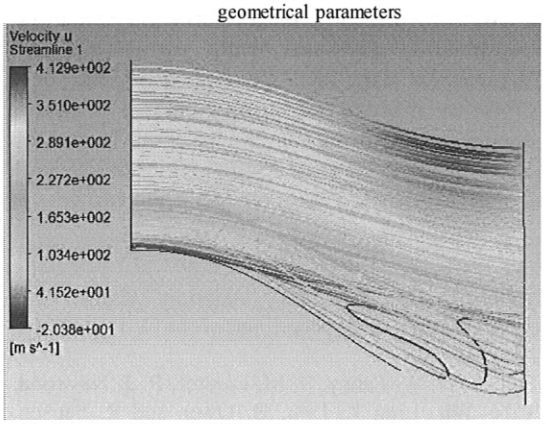

Fig. 23: Streamlines inside the S-duct obtained from testing of geometrical parameters

IX. CONCLUSION

The main goal of the paper was to understand the effects of BLI on the inlet performance on an MF-BWB aircraft and obtain an inlet design that produces minimum total pressure distortion and maximum total pressure recovery at the AIP. Hence, an inlet design that effectively curtails these losses was required. Based on the geometrical parameterization of the

duct, variations in the values of parameters like inlet aspect ratio, duct length, and duct height, were chosen for testing different inlet configurations and understand their effects on the results:

1. The results of the testing on different inlet aspect ratios showed that the pressure recovery was maximum for the aspect ratio of AR=1.75.
2. The inlet with AR=1.75 produced a pressure recovery value of 97.01% but a DC_{60} value of 41.59%, which was quite high for the engine to handle.
3. A higher value of aspect ratio reduced the adverse pressure gradient on the upper wall of the duct due to smaller semi-major axis length of the inlet face. Therefore, the inlet with AR=1.75 was chosen as the one with optimum aspect ratio value and selected for further testing.
4. The lowest DC_{60} value of approximately 33.48% was achieved by the inlet with AR=1 with a pressure recovery value of 96.28%. However, the mass averaged Mach number at the engine fan-face for the duct with AR=1 was 0.66, which is quite high.
5. Results showed that increasing the duct height increased distortion at the AIP and reduced the total pressure recovery. The inlet with the lowest duct height (0.3m) produced most optimum results with a pressure recovery value of 97.7% and a DC_{60} value of 28.45%. Further investigation of other configurations was required to minimize the losses.
6. It was noticed that increasing the duct length reduced the total pressure recovery. It also had an adverse effect on the DC_{60} value.

A conclusion on the aspect ratio, length and height were made (L=4.85m, AR=1.75, H=0.3m) with PR=97.7% and DC(60)=28.45%. So far, this inlet provided the best performance for an embedded engine on a BWB operating in transonic conditions. However, the results could be further improved, hence a number of other configurations of inlet will be tested to understand their effects on inlet performance

REFERENCES

[1]. B. Owen and D. Lee "Aviation Emissions", Encyclopedia of Aerospace Engg., John Wiley &Sons, 2010.

[2]. D. S. Lee, D. W. Fahey, P. M. Forster, P. J. Newtond, R. C.N. Wit, Ling L. Lim, B. Owen and R. Sausen, "Aviation and global climate change in the 21st century", Atmospheric Environment, Vol. 43, 3520–3537, 2009

[3]. Airbus, Navigating the future: Airbus global market forecast 2012-2031, Airbus, 2012

[4]. "Flightpath 2050 Europe's Vision for Aviation", Report of the high level group on aviation research, Publications Office of the European Union, 2011.

[5]. A. Gangoli Rao, F. Yin and J.P. van Buijtenen, "A Hybrid Engine Concept for Multi-fuel Blended Wing Body", Aircraft Engineering and Aerospace Technology, Vol. 86 (6), Sept 2014.

[6]. A. G. Rao, F. Yin and J. P. van Buijtenen, "A Novel Hybrid Engine Concept for Aircraft Propulsion ", The XX international symposium on Air Breathing Engines, Gothenburg, 2011;

[7]. L. Smith Jr., *"Wake Ingestion Propulsion Benefit"*, AIAA/SAE/ASME/ASEE, 27th Joint Propulsion Conference, California, USA, 1991.

[8]. L. Peijian, A. G. Rao, D. Ragni and L. Veldhuis, "Performance Analysis of Boundary Layer Ingestion for Aircraft Design", *Journal of Aircraft*, Vol. 53, issue 5, pp. 1517-1526, 2016;

[9]. K.G. Heinz, and F. Reinhard, "CRYOPLANE: hydrogen fuelled aircraft — status and challenges", Air & Space Europe, Vol. 3, No.3-4, Pages 252-254, May-August 2001.

[10]. R. Slingerland, "Innovative Configurations and Advanced Concepts for Future Civil Aircraft", VKI Lecture Series on Aircraft Design, 2005.

[11]. Callewaert, P., et al., "Multifuel Blended Wing Body", Design Synthesis Exercise Report, TUDelft, the Netherlands, January, 2012

[12]. J. Mattingly, W. Heiser and D. Daley, "Aircraft Engine Design", AIAA Education Series, 1987

[13]. H. Saravanmuttoo, G. Rogers, and H. Cohen, "Gas Turbine Theory", Pearson Education, 2001

[14]. C. Huo, N.G. Diez, and A.G. Rao, "Numerical Investigations on the Conceptual Design of a Ducted Contra-Rotating Fan", Proceedings of the ASME Turbo Expo 2014:

[15]. T. Reichel, S. Terhaar, O. C. Paschereit, "Increasing Flashback Resistance in Lean Premixed Swirl-Stabilized Hydrogen Combustion by Axial Air Injection", J. Eng. Gas Turbines Power 137(7), 071503, 2015

[16]. A.G. Rao and Y. Levy, "A New Combustion Methodology for Low Emission Gas Turbine Engines", proceedings of the 8th HiTACG conference, July 5-8, Poznan, 2010,

[17]. I.P. Van Dijk, A.G. Rao, and J.P. van Buijtenen, "Stator Cooling and Hydrogen Based Cycle Improvements", *Int. Soc. of Air Breathing Engines 2009*, Montreal Canada, ISABE 2009-1165, 2009.

[18]. P. Lv, D. Ragni, T. Hartuc, L. Veldhuis and A. G. Rao, "Experimental Investigation of the Flow Mechanisms Associated with a Wake Ingesting Propulsor", *AIAA Journal*, Vol. 55 (4), pp. 1332-1342, 2017.

[19]. D.L. Daggett, R. Kawai and D. Friedman, "Blended Wing Body System Studies: Boundary Layer Ingestion with Active Flow Control", NASA Langley Research Center, vol. NASA/CR-2003-212670, Virginia, USA, 2003.

[20]. A.P. Plas, M.A. Sargeant, V. Madani, D. Crichton, E.M. Greitzer and T.P. Hynes, "Performance of a Boundary Layer Ingesting Propulsion System", 45th AIAA Aerospace Sciences Meeting and Exhibit, Nevada, USA, 2007.

[21]. A.J. Anabtawi, R. Blackwelder, R. Liebeck, P. Lissaman, "Experimental Investigation of Boundary

Layer Ingesting Diffusers of a Semi-Circular Cross Section", 36th Aerospace Sciences Meeting and Exhibit, Nevada, USA, 1998.

[22]. L.R. Owens, B.G. Allan and S.A. Gorton, , "*Boundary Layer Ingesting Inlet Flow Control*", NASA Langley Research Center, Virginia, USA, 2006.

[23]. A. Rabe, S. Olcmen, J. Anderson, R. Burdissoand and W. Ng, "A Facility for Active Flow Control Research in Serpentine Inlets", 40th AIAA Aerospace Sciences Meeting & Exhibit, Nevada, USA, 2002.

[24]. B.L. Berrier and B.G. Allan, "Experimental and Computational Evaluation of Flush-Mounted, S-Duct Inlets", 42nd AIAA Aerospace Sciences Meeting and Exhibit, Nevada, USA, 2004.

[25]. B.G. Allan, L.R. Owens and B.L. Berrier, "Numerical Modeling of Active Flow Control in a Boundary Layer Ingesting Offset Inlet", 2nd AIAA Flow Control Conference, AIAA-2004-2318, Oregon, USA, 2004.

[26]. A.M. Ferrar, "Measurements of Flow in Boundary Layer Ingesting Serpentine Inlets", Master Thesis, Faculty of The Virginia Polytechnic Institute and State University, Virginia, USA, 2011.

[27]. R.E.C. van Dijk, , "Tools and Methods for Next-Generation Knowledge-Based Engineering Systems", Unpublished Doctoral Dissertation, Delft University of Technology, Delft, The Netherlands, 2018 (to be published).

[28]. ParaPy B.V., "ParaPy – Knowledge Based Engineering Platform", https://www.parapy.nl, last accessed: 09 November 2017.

[29]. A.Sharma "Design of Inlet for Boundary Layer Ingestion in a Blended Wing Body Aircraft", M.Sc. Thesis, Delft University of Technology, 2015.

[30]. B. G. A. Gowda, "Aerodynamic effect of canard on a blended wing body aircraft in transonic regime: A numerical study using SU2", M.Sc. Thesis, Delft University of Technology, 2017.